Equation of State and Radial Distribution Functions of FCC Particles in a CFB

Dimitri Gidaspow and Lu Huilin
Dept. of Chemical and Environmental Engineering, Illinois Institute of Technology, Chicago, IL 60616

Kinetic theory of granular flow was verified experimentally for flow of fluid catalytic cracking particles in a vertical pipe. Measurements of particle pressure using a differential transducer and granular temperature with a digital camera as a function of bulk density, determined using an X-ray densitometer, showed that a relation exists among pressure, temperature, and density, analogous to the ideal gas law. In the limit of zero solids volume fraction: (Solid Pressure)/[(Granular Temperature) × (Bulk Density)] = 1.0. Measurements of radial distribution functions using the digital camera showed that their peak values occur at particle contact and lie between the predictions from the Bagnold equation and Carnahan–Starling equation. The hard sphere model was corrected for a cohesive pressure using the minimum in the measured radial distribution function. The new model agrees with the pressure measurements in the dense regime.

Introduction

In a number of pioneering papers Savage and collaborators (Savage and Jeffrey, 1981; Jenkins and Savage, 1983; Savage, 1983, 1988) showed that dense-phase kinetic theory can be applied to granular flow of particles. This theory, as reviewed by Gidaspow (1994), shows that there exists an equation of state for particles that is a relation among particle pressure, granular temperature, and bulk density. Granular temperature is defined to be one-third the sum of the squares of the random particle oscillations in the three directions. This theory also allows the computation of viscosity of particles from measurements of granular temperature (Gidaspow and Huilin, 1996a; Gidaspow et al., 1995; Shao et al., 1995) or from measurements of granular pressure (Chen et al. 1994). Carlos and Richardson (1968) used a photographic technique to measure particle oscillations in a liquid–solid fluidized bed, while Arastoopour et al. (1992) used a laser Doppler velocity meter to show that the particle-velocity distribution for flow of a dilute solid–gas mixture in a tube is approximately Maxwellian. Gidaspow et al. (1995) and Bahary (1994) developed a digital camera technique to measure the granular temperature. Cody et al. (1995) developed an acceleration probe and a method of measuring granular temperature in commercial fluidized beds by Fourier analysis of noise. Campbell and Wang (1990, 1991) and Campbell and Rahman (1992) developed a clever method of measuring the small-particle pressure. Their technique is used in this study. Despite the availability of techniques to measure the basic variables, there exists no experimental verification of kinetic theory of granular flow.

Flow of dense suspensions was recently reviewed by Jackson in a plenary lecture (1993). Crowe et al. (1996) reviewed the more dilute two-phase flow. The theory of granular flows has been developed in a number of other excellent papers (e.g., Lun et al., 1984; Jenkins and Richman, 1985; Campbell, 1989; Richman, 1989; Rhodes, 1990; Rogers and Eaton, 1991; Sommerfeld, 1992; Pita and Sundaresan, 1993; Simonin et al., 1993; Brady, 1994; Eaton, 1994; Massoudi and Ahmadi, 1994; Viollet and Simonin, 1994; Cao and Ahmadi, 1995; Tsao and Koch, 1995; Glasser et al., 1996; Sangani et al., 1996; Phung et al., 1996).

This article shows that there indeed exists an equation of state for particles analogous to the ideal gas law for dilute flow. For dense flow there is considerable deviation that can be only partially explained by the collisional finite-volume-type contribution in the theoretical equation of state. The experimental equation of state was obtained by measuring particle pressure with the transducer described in this article and by measuring the granular temperature with a video digital camera technique as a function of particle volume fraction described earlier by Gidaspow and Huilin (1996a). It com-

Table 1. Particle-Size Distribution

d_p (μm)	% Particle (Miller and Gidaspow, 1992)	d_p (μm)	Fraction
5.936—8.0	0.275	0.0—30.0	0.0644
8.0—12.0	0.710	30.0—53.0	0.1221
12.0—16.0	0.311	53.0—75.0	0.4083
16.0—20.0	0.495	75.0—106.0	0.3059
20.0—40.0	4.545	106.0—150.0	0.0646
40.0—80.0	50.67	150.0—177.0	0.0233
80.0—100.0	27.215	177.0—200.0	0.0024
100.0—140.0	12.314		
140.0—200.0	1.407		
200.0—400.0	1.399		
400.0—572.2	0.651		

pares reasonably well to a hard sphere model corrected for a cohesive pressure estimated from measurements of radial distribution functions.

The equation of state was for 75 μm (Table 1 shows the particle-size distribution) fluid catalytic cracking (FCC) particles. They are used in the oil industry to make gasoline from oil. Squires et al. (1985) described FCC powder as somewhat like cement powder but much more freely flowing. The tests were conducted in the vertical tube of a two-story circulating fluidized bed (CFB) apparatus shown in Figure 1. Miller and Gidaspow (Miller and Gidaspow, 1992; Miller, 1991) had previously obtained radial particle concentration and flux profiles in this apparatus. Figure 2 shows a typical particle concentration profile and the location of measurements. From such data and pressure-drop measurements, Miller and Gidaspow (1992) computed the FCC viscosity as a function of particle volume fraction. This viscosity was recently found to agree with the viscosity obtained using kinetic theory computed from granular temperature measurements (Gidaspow and Huilin, 1996a). Elghobashi (1994) and Crowe et al. (1996) show the different regimes of particle turbulence in a dilute gas–solid flow system. The particles respond primarily to the

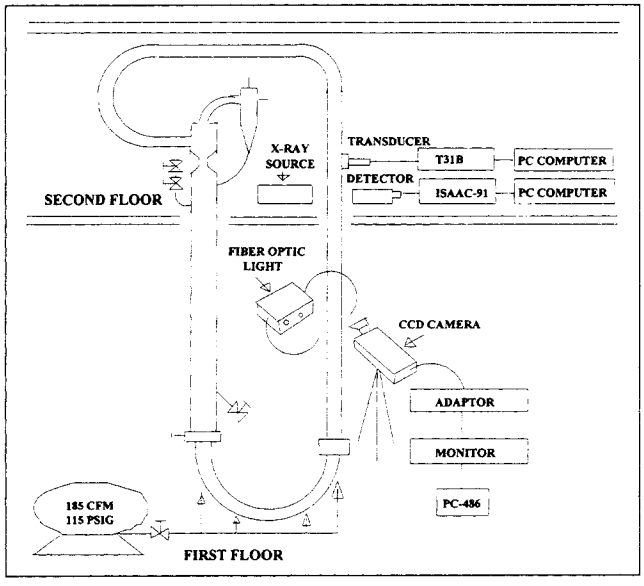

Figure 1. IIT circulating fluidized bed with particle pressure transducer, CCD camera, and X-ray densitometer.

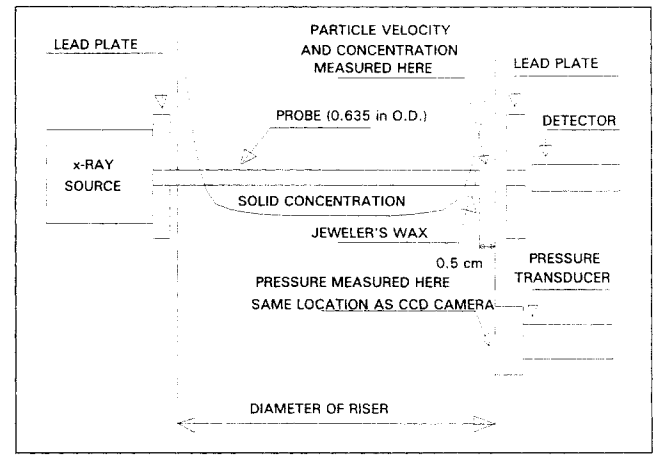

Figure 2. Determination of particle concentrations in this study (Miller and Gidaspow, 1992).

gas-phase turbulence at very low solid-volume fractions (Elghobashi and Abou-Arab, 1983), while at the higher solid-volume fractions particles experience velocity fluctuations induced by interparticle collisions (Louge et al., 1991). For the gas–solid flow of 75-μm FCC particles, Table 2 lists typical values of the Reynolds number $Re = (U_g d_p \rho_g)/\mu_g$, the Stokes number $St = \rho_s d_p^2 \gamma/(18\mu_g)$, the Bagnold number $N_{\text{Bagnold}} = \rho_s d_p^2 \gamma/\mu_g$, and the dimensionless group $R = d_p\gamma/(4\theta^{0.5})$. Experimental data presented in this article can be used for verification of various theories being developed using analytical (Sinclair and Jackson, 1989) or molecular dynamic simulations (Ahn and Brennen, 1993; Tsuji et al., 1993; Tanaka et al., 1993; Yonemura et al., 1993; Walton and Braun, 1986; Walton, 1993).

Particle-Pressure Transducer and X-Ray Densitometer

A particle-pressure transducer that is capable of resolving the particle pressure independently of the fluid pressure was first built by Campbell and Wang (1990, 1991). Kumar et al. (1990) used a hydrophone to measure the granular pressure in liquid–solid fluidized beds. Chen et al. (1994) continued the work of Campbell and Wang (1990, 1991) and used the measurements of particle pressure to obtain powder viscosity.

Particle-pressure transducer

The particle pressure was measured using a differential pressure transducer PDCR made by Druck Incorporated (see Figure 3). The operating principle of the pressure transducer is as follows. The front of the diaphragm of the pressure

Table 2. Typical Values of Reynolds Number, Stokes Number, and Bagnolds Number for 75 Micron FCC Particles in CFB

ϵ_s	γ (1/s)	Re^*_{particle}	St	R	N_{Bagnold}
0.05	300	10.71[1]	9.21	0.004[1]	165.8
0.10	400	16.07[2]	12.28	0.006[2]	221.0
0.20	470	21.43[3]	14.43	0.011[3]	259.7

*1—U_g = 2.0 m/s, θ = 2.0 (m/s)^2; 2—U_g = 3.0 m/s, θ = 1.5(m/s)^2; 3—U_g = 4.0 m/s, θ = 0.6 (m/s)^2.

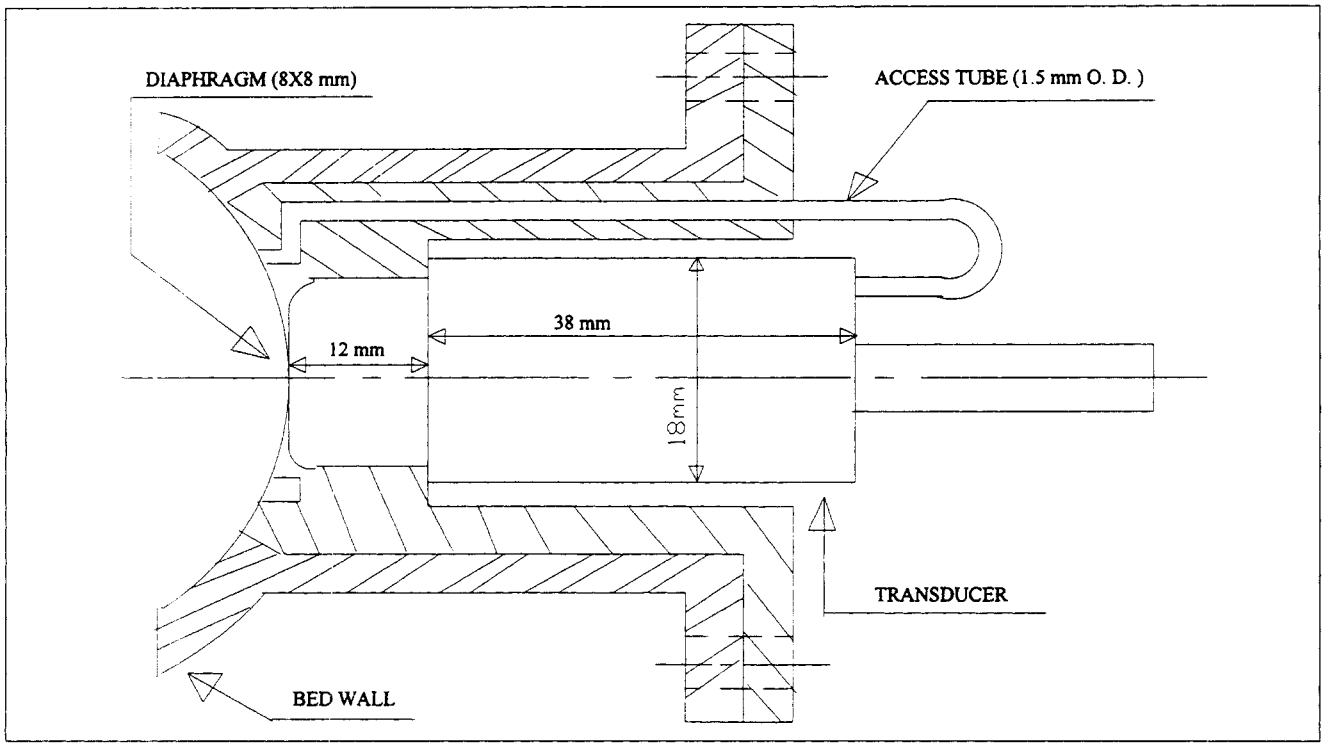

Figure 3. Particle pressure transducer.

transducer, which was mounted flush with the bed wall, experienced the combined forces of the gas and particle phase. Small passages about the circumference of the diaphragm admit air but no particles. Thus, the front of the diaphragm experiences both gas and particle pressure, and the back experiences only gas pressure, so that the net deflection of the diaphragm reflects the pressure exerted on the surface by particle interactions. Since in fact the gas-pressure fluctuations take a finite amount of time to reach the rear of the diaphragm, the instantaneous pressure detected by the transducer might be different from the actual solid pressure. However, its time-averaged response should correspond to the time-averaged solid pressure (Campbell and Wang, 1990, 1991; Campbell and Rahman, 1992). In addition, a test suggested by Campbell and Wang (1990, 1991) was performed to verify that the gas pressure can be canceled out, at least on a time-averaged basis. Thus, the signal from the pressure transducer is averaged over long time periods to yield the average particle pressure.

Preliminary experiments showed that the placement of the gas ports surrounding the diaphragm could be critical. In a quiescent fluid this is not a problem because the fluid pressure is uniform across the face of the diaphragm. Difficulties arise if there is a pressure gradient tangential to the diaphragm surface. In this case, the fluid could tend to enter a port where the pressure is large and leave through another port where the pressure is lower. This could present a particular problem when the pressure drop is large so that the path through the transducer is easier than that on the outside. To avoid this difficulty, our pressure transducer has only two fluid-pressure input ports, one located on either side of the diaphragm along a diameter oriented perpendicular to the pressure gradient. These input ports were covered with a thin membrane that had 10 holes of 40 μm diameter at each side. In this way, the pressure difference between the ports is zero. No flow is induced across the interior of the transducer; also no particles entered the rear tube of the transducer.

X-ray densitometer

The X-ray densitometer used by Miller (1991) and Miller and Gidaspow (1992) measured the particle concentration. Figure 2 shows a sketch of the probe extending into the pipe region. Some pertinent details are as follows: the source of the X-ray densitometer is a 200-mCi Cu-244 source having 17.8 half-life. It emitted X-rays with a photon energy between 12 and 23 keV. The source was contained in a ceramic enamel, recessed into a stainless-steel support with a tungsten alloy packing, and sealed in a welded Monel capsule. The intensity of the transmitted X-ray beam was detected by an NaI crystal scintillation detector. It consisted of a 2-mm-thick, 5.08-cm-diameter tube with a 0.13-mm-thick beryllium window. The photomultiplier of the detector was connected sequentially to a preamplifier, an amplifier, and a double-channel analyzer. The attenuation coefficient for the 75-μm FCC particles was found to be 0.08133 cm^2/g. A calibration curve was obtained by measuring radiation counts for an empty tube and one filled with particles. At a solid volume fraction, 0.6, the average count was 16,100 per second, while for the empty tube it was 19,600 per second.

Particle Pressure

Typical results of variation of particle pressure with time are shown in Figure 4. We determined the influence of the

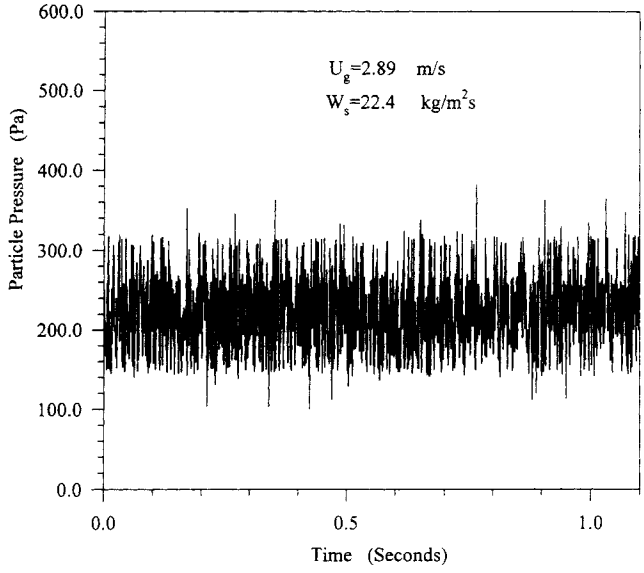

Figure 4. Instantaneous particle pressure in dilute regime.

sampling frequency on the time-average particle pressure. At 1500 Hz there was no influence.

The influence of solid mass flux on time-average solid pressure is shown in Figure 5. Solid pressure increases with increasing solid mass flux, as expected. Table 3 summarizes the experimental data. The solid pressure increases monotonically with solid-volume fraction in the range of measurement, as shown in Figure 6.

Granular Temperature

The granular temperature was measured by means of the high-resolution micro/measuring system shown in Figures 1 and 2 (Gidaspow and Huilin, 1996a). It was first used by Bahary (1994) and by Gidaspow et al. (1995) for measurements in a three-phase fluidized bed. The system consists essentially of two units: a high-resolution microimage system and a data-managing system. The high-resolution microimage system is a 2/3-in. (17-mm) color video camera (DXC-151A) that uses a charge-coupled device (CCD), a solid-stage image sensor. This camera has ten electronic shutter settings and four modes for gain control. The horizontal resolution of the camera is 460 TV line, and a sensitivity of 2,000 lux at 0 dB for gain. The camera adapter is a Sony CMA-D2 that connects the camera to a 486/33-MHz IBM computer. The personal

Table 3. Summary of Experimental Solid-Pressure Data

U_g (m/s)	W_s (kg/m^2·s)	ϵ_s	P_s (Pa)
2.89	8.86	0.00651	8.86
2.89	9.98	0.00835	9.98
2.89	10.05	0.00867	10.05
2.89	11.37	0.01034	11.37
2.89	16.09	0.02301	27.11
2.89	19.03	0.0284	63.95
2.89	20.89	0.0383	105.62
2.89	24.33	0.0521	253.39
2.46	29.57	0.0855	469.13
2.46	27.06	0.1134	446.06
2.46	21.79	0.0616	202.76
2.46	20.36	0.0470	146.92
2.46	18.26	0.0387	108.69
2.89	13.95	0.1015	413.22
2.89	14.57	0.1097	435.31
2.89	16.79	0.1106	444.64
2.89	17.59	0.1355	476.08
2.89	21.35	0.1531	501.96
2.89	28.27	0.1959	521.03
2.89	30.95	0.2224	546.46
2.14	15.54	0.1325	489.93
2.14	20.51	0.1591	540.13
2.14	23.44	0.1739	541.24
1.60	18.19	0.1949	511.19
1.60	20.64	0.2146	555.03
1.60	25.78	0.2357	564.56

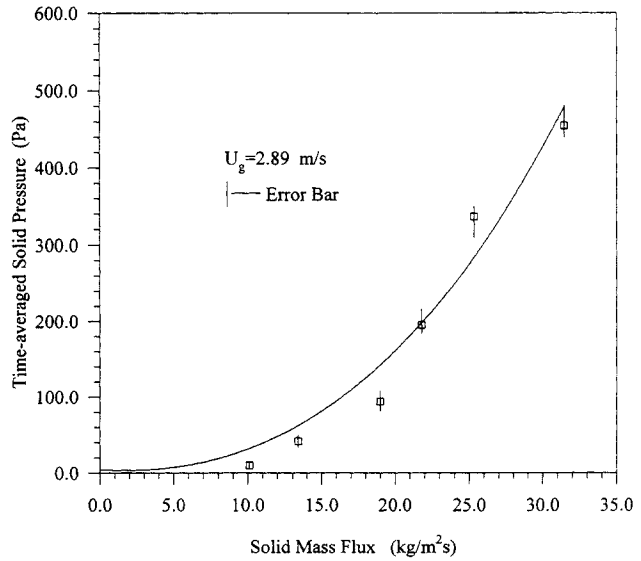

Figure 5. Effect of solid-mass flux on the time-averaged solid pressure.

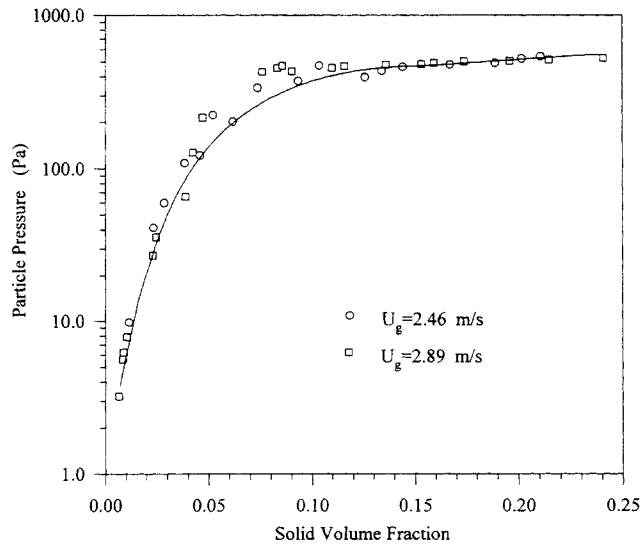

Figure 6. Time-averaged solid pressure in IIT CFB.

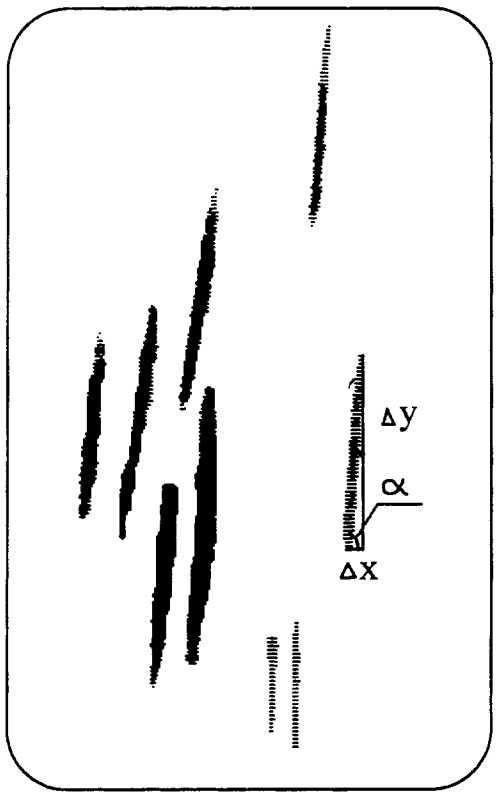

Figure 7. Streak images captured by the CCD camera recording system for flow of 75-μm FCC particles in the IIT CFB.

This figure shows a small portion from the screen on which images are captured; e.g., $\Delta y = 1.44$ mm; $\Delta x = 0.22$ mm; $\alpha = 80°$; $\Delta t = 0.5$ ms.

computer has a microimaging board and a microimaging software, Image-Pro Plus, for data measurement and analysis.

For good visualization of microscopic movement of particles, a fiber-optic light was used. The area of view in most experiments was a 5×20 mm. As the particles were fluidized inside the riser, the camera with a zoom lens, 18–108 mm, and close-up focus transferred its field of view into the monitor. Figure 7 shows a typical streak made by the particles. These streak lines represent the distance traveled by the particles in a given time interval specified on the camera. The images were then captured and digitized by the Image-Pro Plus software. To obtain reliable velocity information, the time between exposures must be selected so as to obtain a sufficient displacement to achieve an acceptable velocity resolution, but must not be so large that the particle moves out of the field of view. The local velocity is then estimated by dividing the distance by time, as shown in Figure 7. Two-dimensional velocity components, tangential and vertical, were determined. Gidaspow and Huilin (1996a) had given typical histograms of velocity distributions.

Variances of velocity were calculated using the standard equation of statistics.

$$\sigma_i^2 = \frac{1}{N} \sum_{i=1}^{N} (v_i - v_m) \qquad (1)$$

Table 4. Granular Temperature Data for Flow—In the Ideal Particle-Law Regime

No.	U_g (m/s)	W_s (kg/m^2·s)	ϵ_s	U_{av} (cm/s)	σ_θ (cm/s)	σ_z (cm/s)	θ (m/s)^2
1	2.89	19.03	0.0284	−18.20	19.45	198.29	1.33
2	2.89	20.89	0.0383	−31.26	15.83	213.36	1.54
3	2.89	24.33	0.0521	−52.53	23.33	258.74	2.27
4*	2.89	4.380	0.0042	274.04	6.773	61.750	0.13
5	2.35	29.35	0.0924	−69.35	16.19	311.89	3.26
6*	2.46	9.704	0.0025	235.35	11.49	75.928	0.21
7	2.46	20.36	0.0470	−31.02	32.78	222.22	1.72
8	2.46	29.57	0.0855	−76.02	21.08	285.38	2.74

*At low solid fluxes, W_s, there is no particle downflow. Frequently (Miller and Gidaspow, 1992) in the CFB flow the particles in the annular region (see Figure 1*b*) flow down as indicated in this table, while the particles in the core region flow up with velocities that exceed the superficial velocity, U_g, shown in the table.
$\theta = (2/3)\sigma_\theta^2 + (1/3)\sigma_z^2$. It is assumed that $\sigma_\theta = \sigma_r$, since flow is primarily in the z = diretion.

where v_i is the velocity in the i direction and v_m is the mean. Shao et al. (1995) have used a similar procedure to calculate the fluctuating velocity using a laser Doppler anemometer. Table 4 contains a summary of the data. The apparatus was constructed to operate as close as possible in the developed flow regime. Ideally in such a situation there is no flow in the radial or tangential directions. Figure 7 shows that this has been nearly achieved. The velocity components in the r- and θ-directions are small compared to the z-direction, the vertical direction. Hence the variance in the θ-direction, as shown in Table 4, is about one-tenth that in the principal direction of the flow. It is therefore reasonable to assume that the r and θ variances are equal. Hence we compute the granular temperature as

$$\theta = \frac{1}{3}(\sigma_\theta^2 + \sigma_r^2 + \sigma_z^2) = \frac{2}{3}\sigma_\theta^2 + \frac{1}{3}\sigma_z^2. \qquad (2)$$

The flow conditions were similar to those of Miller and Gidaspow (1992). Note that the granular temperature was measured 5 mm from the wall, while the solid pressure was measured flush with the wall. The anisotropy of the velocity fluctuations is a strong function of the position, since granular temperature and the mean velocity are strongly correlated, as observed experimentally.

Radial Distribution Function Measurement

Radial distribution functions play a key role in the statistical mechanics of liquids (e.g., Hansen and McDonald, 1991). They are often measured using neutron scattering techniques. Light scattering techniques were used at the Illinois Institute of Technology to obtain radial distribution functions of colloid particles (Wasan et al., 1996; Xu et al., 1996). Earlier fluorescence microscopy and quasielastic light-scattering measurements were used to determine the radial pair distribution functions of acrylic spherical suspensions (Yoshida et al., 1990; Leighton and Rampall, 1993).

We used our CCD camera system to measure the local particle distributions. Figure 8 shows a typical particle-distribution image for 75-μm FCC particles, approximately at the same location as the particle-volume fraction, granular tem-

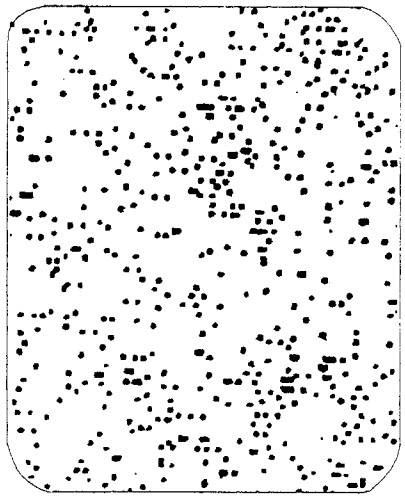

Figure 8. A small portion of an image of particle distribution captured by CCD camera for 75-μm FCC particles.

Gas Velocity = 2.46 m/s; solid mass flux = 18.44 kg/m^{2}s.

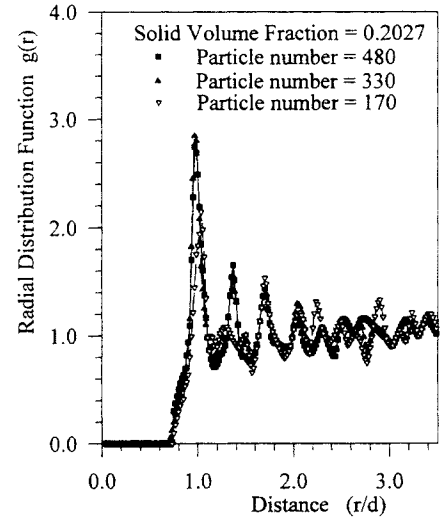

Figure 10. Effect of particle count on the radial-distribution-function profile.

U_g = 2.89 m/s; W_s = 27.71 kg/m^{2}s.

perature, and particle-pressure measurements. The CCD camera system stores the coordinates of each particle in the image, such as shown in Figure 8. Its center position and area were determined by software IPPLUS and stored in a computer. The radial distribution function $g(r)$ was calculated as follows (Balucani and Zoppi, 1994; Egelstaff, 1967; Hunter, 1989):

$$\Delta N = 2\pi \bar{r} \frac{N}{\text{AREA}} g(\bar{r}) \Delta r, \tag{3}$$

where N is the total particle number in the AREA, and ΔN is the particle number in the computing area. This method is very similar to the Monte Carlo simulation of the equation of state (Temperley et al., 1968; Hail and Mansoori, 1983). The "termination effect" was eliminated by the method described by Yoshida et al. (1990). This boundary-condition treatment is different from the periodicity assumption in molecular simulations (Metropolis et al., 1953). Figure 9 summarizes the concept of the radial distribution function and its calculation. Figure 10 shows the effect of the particle count number of the inner circle on the radial distribution function. In our computation of the radial distribution function, the area of the inner circle must contain no less than 300 particles. Figure 11a and 11b show the typical radial distribution function profiles for flow of 75-μm FCC particles in our riser shown in Figure 1. Compared with the hard-sphere model, we have nonzero values below the mean particle diameter because of the particle-size distribution. From these figures, the radial distribution function g_o at contact, $r = d$ (mean particle diameter) was determined. Figure 12 shows the comparison of the experimental data with computed results as a function of solid-volume fraction using Bagnold's and Carnahan and Starling's equations. We see that the Bagnold equation we used previously (Gidaspow and Huilin, 1996a) agrees approximately with the data. A possible cause for the measured data being larger than that of Carnahan and Starling results is that the particle-size distribution is not uniform. The Carnahan

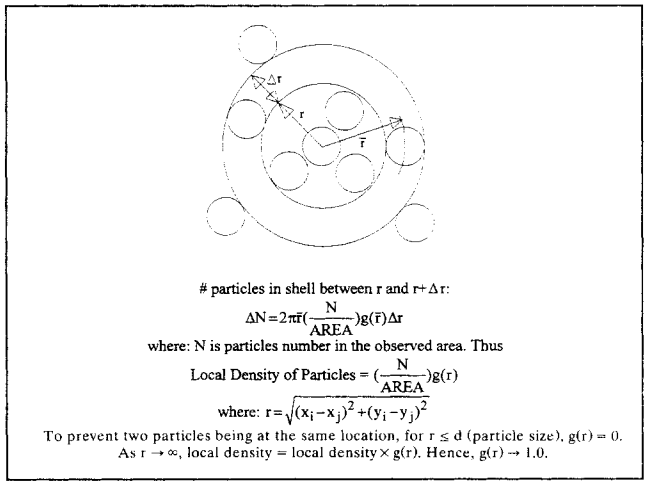

Figure 9. Concept of radial-distribution function.

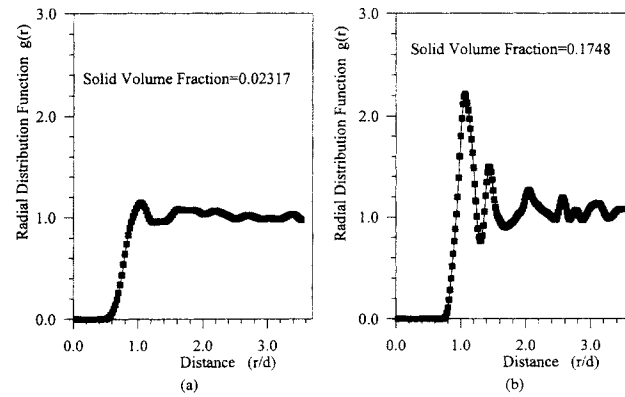

Figure 11. Radial-distribution-function profile.

(a) U_g = 2.67 m/s; W_s = 12.62 kg/m^2·s; (b) U_g = 2.67 m/s; W_s = 27.44 kg/m^2·s.

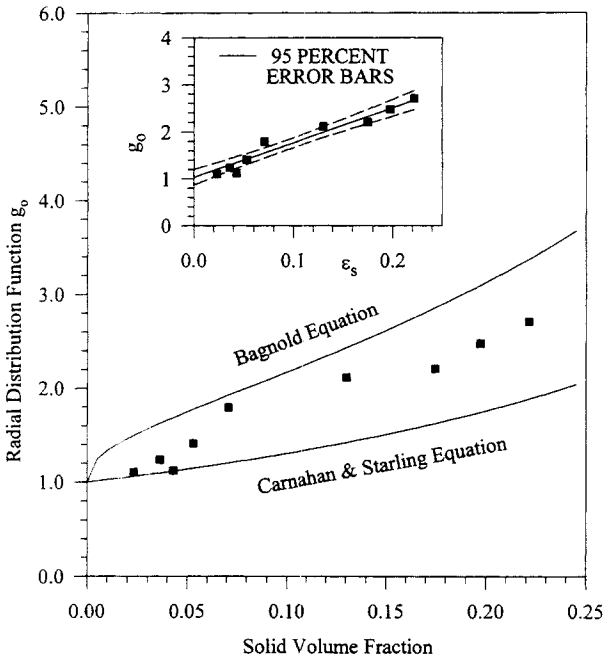

Figure 12. Measured and computed radial-distribution function at particle contact (Bagnold Eq.: Eq. 6 in text; Carnahan and Starling Eq.: Eq. 15 in text).

and Starling equation is only suitable for monodisperse hard spheres. Simulations of binary mixtures show that the radial distribution function of a mixture of fines and large particles can have a distribution function at contact for the large particles many times that of large particles alone. The shell next to the large particle will have many small particles (Chu et al., 1996a).

Comparison to Kinetic Theory

Solids pressure

Lun et al. (1984) and Lun and Savage (1987) obtained a relation between the solid pressure, p_s, and the granular temperature, θ, using the methods of dense-phase kinetic theory. Gidaspow (1994) has reviewed this derivation using the classic Chapman and Cowling's (1961) method. The expression given below includes a kinetic contribution, which is like the ideal gas law, and a collisional contribution that is like the van der Waals kinetic volume constant, b, modified by the particle restitution coefficient e:

$$p_s = \epsilon_s \rho_s \theta [1 + 2\epsilon_s (1+e) g_0]. \tag{4}$$

Since in our experiment, the restitution coefficient is nearly unity, as estimated by Gidaspow (1994) and confirmed for dilute flow in Appendix A, Eq. 4 is simply the hard-sphere model of statistical mechanics (Hansen and McDonald, 1991):

$$\frac{\beta p}{\rho} = 1 + 4\epsilon_s g_o. \tag{5}$$

In Eq. 5, β is the reciprocal of the granular temperature and ρ is the bulk density, $\epsilon_s \rho_s$. A simple form for the radial distribution function, g_o, is that used by Bagnold (1954), as reviewed by Gidaspow (1994):

$$g_0 = \left[1 - \left(\frac{\epsilon_s}{\epsilon_m}\right)^{1/3}\right]^{-1}. \tag{6}$$

Note that since in Eq. 4 the restitution coefficient enters as $(1+e)$ the precise value of e is not important. However, for modeling the observed radial volume fraction and velocity distributions in our riser Samuelsberg and Hjertager (1996) used $e = 0.995$. In work in progress (Gidaspow et al., 1997), we determine the restitution coefficients of FCC particles from a ratio of measured Reynolds stresses to granular temperature to be again close to unity.

The pressure data shown in Figure 6 were converted to the granular temperature using Eqs. 4 and 6 ($\epsilon_m = 0.636$). Figure 13 shows a comparison of the measured and computed granular temperature. This figure also shows the calculated granular temperature using the Carnahan and Starling (1969) equation of radial distribution function g_o. Both sets of data are very similar, as already shown by Gidaspow and Huilin (1996a).

Granular temperature

The granular temperature rises rapidly with solid-volume fraction, reaches a maximum near a solid-volume fraction of about 6%, and then decreases slowly, see Figure 13. Such behavior is reasonable since the granular temperature is zero with no particles and will approach zero for a packed bed, in which there is no particle motion. The figure also shows the granular temperature computed from the viscosity measured

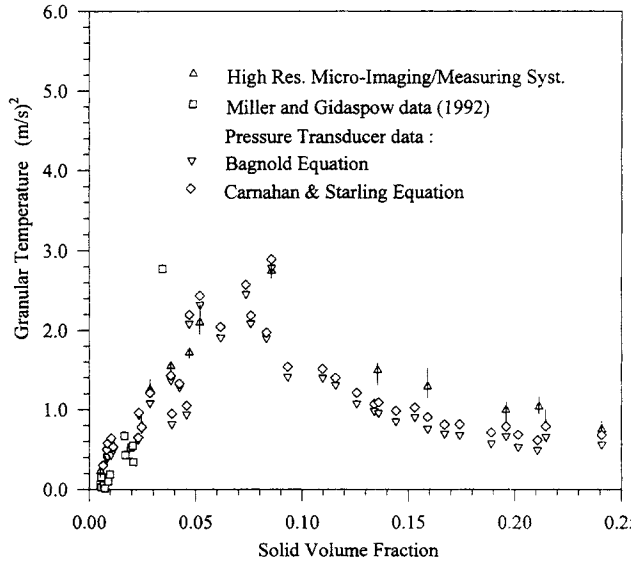

Figure 13. A comparison of granular temperature computed from particle pressure to direct measurements using CCD camera (Gidaspow and Huilin, 1996) and granular temperature from viscosity measurements (Miller and Gidaspow, 1992).

by Miller and Gidaspow (1992) from gas pressure-drop shear data, using the kinetic-theory viscosity relation:

$$\mu_s = \frac{5\rho_p d_p\sqrt{\pi\theta}}{48(1+e)g_0}\left[1+\frac{4}{5}(1+e)g_0\epsilon_s\right]^2 + \frac{4}{5}\epsilon_s^2\rho_p d_p g_0(1+e)\sqrt{\frac{\theta}{\pi}} \quad (7)$$

reported by Gidaspow (1994). This expression is nearly identical to that of Lun et al. (1984) and Lun and Savage (1987).

Recently, Tsao and Koch (1995) suggested the concept of the quenched state in which the viscous relaxation time is less than the collision time and postulated an ignited state for dilute suspensions. They found that the granular temperature increases with increasing solid-volume fraction in the quenched state, but decreases in the ignited state. They claim to have solved the problem of the mathematical singularity in the limit of $\epsilon_s \to 0$. Here we show that such a singularity arises from the assumption of incompressibility deleted in their analysis.

In the dilute flow without particle collisions, the mass, momentum, and energy equations for the particulate phase, as a first approximation, using the Maxwellian velocity distribution, are (e.g., Lun et al., 1984; Lun and Savage, 1987; Gidaspow, 1994):

$$\frac{D\epsilon_s}{Dt} = -\epsilon_s\frac{\partial \boldsymbol{v}}{\partial \boldsymbol{r}} \quad \text{(constant } \rho_s \text{ conservation of particles)} \quad (8)$$

$$\frac{D\bar{\boldsymbol{v}}}{Dt} = -\frac{1}{\epsilon_s\rho_s}\frac{\partial \boldsymbol{p}}{\partial \boldsymbol{r}} \quad \text{(inviscid particle momentum balance)} \quad (9)$$

$$\frac{3}{2}\epsilon_s\rho_s\frac{D\Theta}{Dt} = -\epsilon_s\rho_s\frac{\partial \boldsymbol{v}}{\partial \boldsymbol{r}} \quad \text{(kinetic energy balance with no dissipation).} \quad (10)$$

Combination of the energy conservation equation (Eq. 10) with the conservation of the mass equation (Eq. 8), gives

$$\frac{3}{2\theta}\frac{D\theta}{Dt} = \frac{1}{\epsilon_s}\frac{D\epsilon_s}{Dt}. \quad (11)$$

This equation shows that the granular temperature, θ, is proportional to the two-thirds power of the solid-volume fraction, as shown below:

$$\theta \propto \epsilon_s^{2/3}. \quad (12)$$

Equation 12 is analogous to the isentropic temperature variation with density for an ideal gas. Such an assumption is a good first approximation in design of compressors and particularly expansion devices. Equation 12 suggests that the granular temperature in Figure 13 rises with the solid volume fraction due to the compression effect. Hence, the viscosity in the dilute limit will rise as $\epsilon_s^{1/3}$. It will not give the infinite value at $\epsilon_s = 0$ obtained in the incompressible shear flow solution. There is no singularity.

For dense suspensions with no dissipation in the fluid and by the wall, the production-dissipation balance gives an equation for granular temperature as (Savage, 1983; Gidaspow, 1994)

$$(1-e^2)^{1/2}\theta^{1/2} = \left(\frac{5\pi}{18}\right)l\left(\frac{\partial u_s}{\partial y}\right). \quad (13)$$

As the mean free path, l, decreases with a higher volume fraction, the granular temperature drops. Equations 12 and 13 explain the behavior of Figure 13.

Equation of state for 75- μm particles

The top of Figure 14 shows that the measured granular pressure, granular temperature, and the solid-bulk volume give essentially the kinetic theory equation of state (Eq. 4). For dilute flow the top of Figure 14 shows that in the limit of zero volume fraction

$$\frac{p_s}{\epsilon_s\rho_s\theta} \cong 1, \quad (14)$$

with an error of 3%. An error analysis is shown in Appendix B. In other words, we have the analogy of the ideal gas law. At volume fractions of solid well above 5%, there is a deviation from ideality that cannot be explained by the collisional

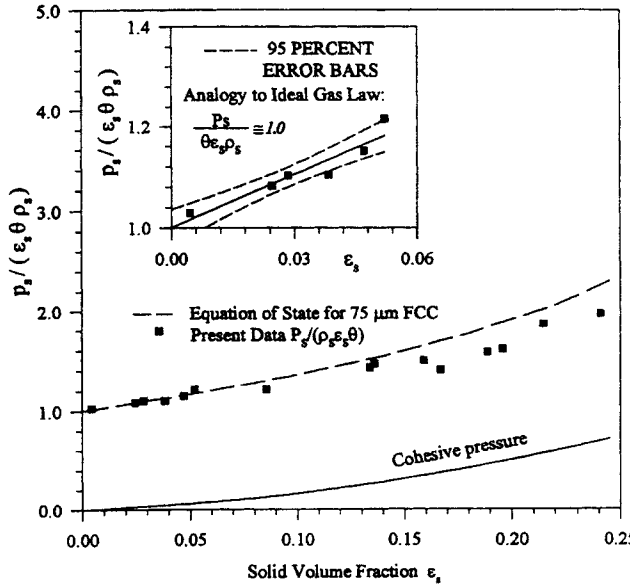

Figure 14. Equation of state for FCC particles determined in IIT CFB:

$$\frac{P}{\rho_s\epsilon_s\theta} = 1 + \underbrace{2(1+e)\epsilon_s g_0}_{\text{Collisional Part}} - \underbrace{(0.73\epsilon_s + 8.957\epsilon_s^2)}_{\text{Cohesive Part}}.$$

Kinetic Part

volume correction given in Eq. 4. Bagnold's expression for the radial distribution function g_0, as given by Eq. 6 gives predictions of pressure that are too high. Carnahan and Starling (1969) equation

$$g_0 = \frac{1}{1-\epsilon_s} + \frac{3\epsilon_s}{2(1-\epsilon_s)^2} + \frac{\epsilon_s^2}{2(1-\epsilon_s)^3} \tag{15}$$

also overpredicts the pressure, as suggested by Savage (1988).

The FCC catalyst differs from ideal particles to which the hard-sphere model is applicable in two essential ways: (1) it is polydispersed (see Table 1); (2) it carries a surface charge. Our measurements using our Faraday cage show that the 75-μm FCC particles carry a small negative surface charge of $1.0\times10^{-4} \sim 3.0\times10^{-4}$ C/kg. This particle surface charge was determined using the measurement system of Gupta (1990) and Gupta et al. (1993).

To determine the effect of these variables, we compare the radial distribution function and its derived quantities to the radial distribution function of monodispersed 450-μm glass beads fluidized in water that have a negligible surface charge (Gidaspow and Huilin, 1996b). Figure 15a shows a typical distribution function at a high solid loading. In liquids the maximum value of the distribution function is not at particle contact, due to a film of liquid that gives rise to a lubrication force. Otherwise, the peak value of the distribution function again lies between that predicated by the Carnahan and Starling and the Bagnold equations, similar to that shown for FCC particles in Figure 12. The principal difference is that for 450-μm glass beads the values of the radial distribution functions never fall below one after the first peak; hence, the potentials, as defined below and shown in Figure 15b, are always negative after the first peak. This potential, W, was calculated from the Boltzmann relation used widely in the molecular theory of liquids (Egelstaff, 1967; Balucani and Zoppi, 1994) and in colloid science (Hunter, 1989). For the Boltzmann constant times the thermal temperature we have substituted the granular temperature, θ, which is the oscillating energy per unit mass of particles:

$$W(r) = -\theta \log[g(r)]. \tag{16}$$

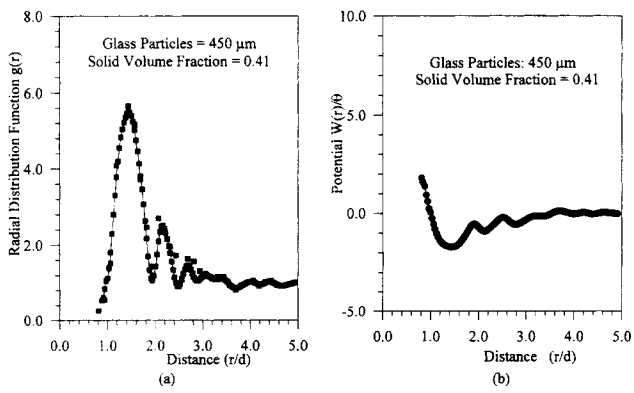

Figure 15. Profiles of radial-distribution function and potential of mean force as a function of solid volume fraction for 450-μm glass particles in a liquid–solid fluidized bed.

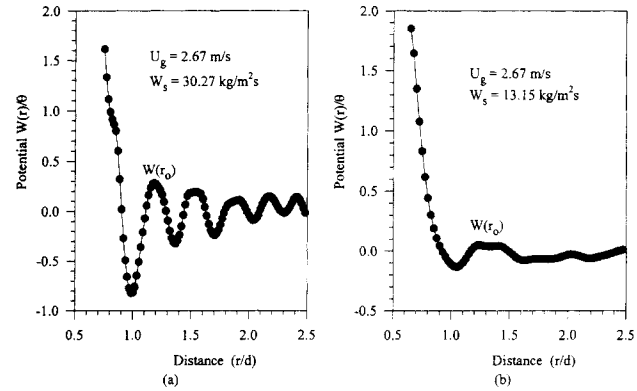

Figure 16. Variations of potential of mean force with dimensionless distance.

Figure 16a and 16b show typical profiles of this potential for FCC particles divided by the granular temperature as a function of dimensionless distance. In these figures, $W(r_o)$ is named the structural energy barrier in colloid science (Chu et al., 1996a,b).

Figure 17a and 17b show the variations of the force with dimensionless distance for 75-μm FCC particles (Balucani and Zoppi, 1994; Hunter, 1989):

$$F(r) = -\frac{d[W(r)/\theta]}{dr}. \tag{17}$$

This force has its maximum value at r_0 and a minimum at particle contact, $r = d$. In colloid science they are called "structural force" and "depletion force," respectively. At r_0 the potential is positive for FCC particles. It is negative for 450-μm glass beads. Figure 18 shows this potential $W(r = d, \epsilon_s)$ as a function of solid volume fraction. If we approximate the measured potential $W(r = d, \epsilon_s)$ by a Dirac delta function at contact, then the first peak of the radial distribution function gives the second term of the equation of state, the collisional portion, as follows:

$$\frac{P_{\text{col}}}{\rho_s \epsilon_s \theta} = -\epsilon_s \frac{d[W(d,\epsilon_s)/\theta]}{d\epsilon_s} = 9.33\epsilon_s^{1.22}. \tag{18}$$

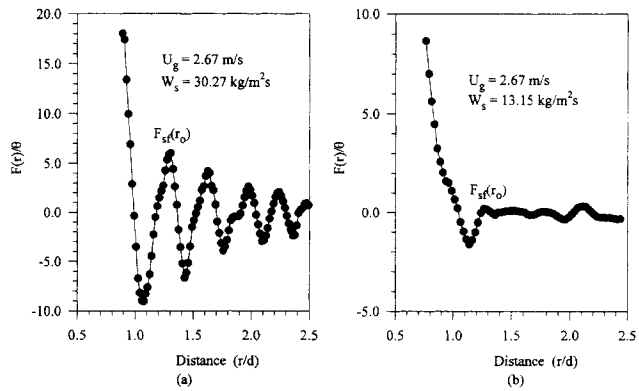

Figure 17. Dimensionless forces for FCC particles.

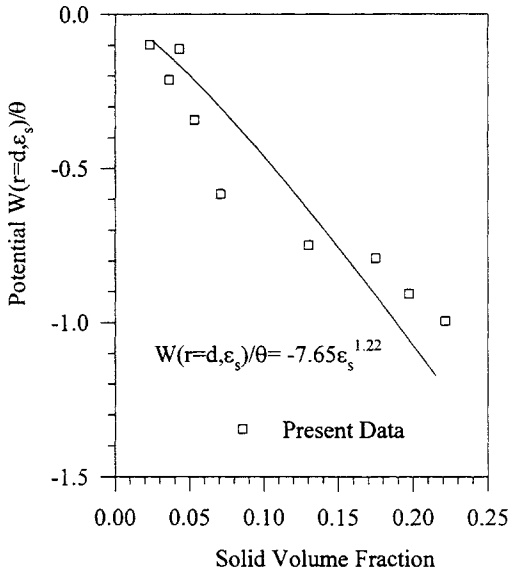

Figure 18. Variation of potential with solid-volume fraction for FCC particles.

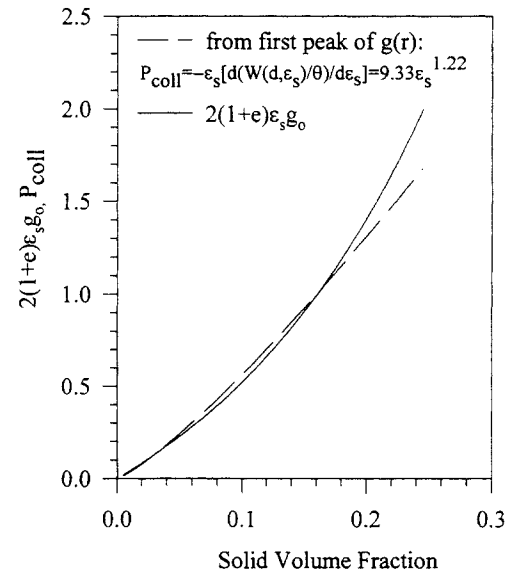

Figure 19. A comparison between the predicted collisional portion and experimental data in the equation of state.

Figure 19 shows the comparison between predictions from Eq. 18 and the collisional portion of Eq. 4 using the restitution coefficient $e = 0.999$. We see that the collisional pressure calculated from the derivative of potential, W, and that obtained from the first peak are the same. Hence we can use the second method for further analysis.

Figure 20 shows the potential $W\ (r = r_0,\ \epsilon_s)$ as a function of solid volume fraction. The derivative of this Helmholtz-type potential at a constant granular temperature is an excess or cohesion pressure, defined as

$$\frac{\partial W(r_0, \epsilon_s)}{\partial(\epsilon_s \rho_s)^{-1}} = P_{\text{cohesion}}. \tag{19}$$

It is related to the slope of the curve in Figure 20 by

$$-P_{\text{cohesion}} = \epsilon_s^2 \rho_s \frac{dW(r_0, \epsilon_s)}{d\epsilon_s}. \tag{20}$$

The solid pressure then becomes:

$$P = P_{\text{kin}} + P_{\text{col}} + P_{\text{cohesion}} = \rho_s \epsilon_s \left[1 + 2(1+e)\epsilon_s g_0 - \epsilon_s \frac{d[W(r_0, \epsilon_s)/\theta]}{d\epsilon_s}\right]\theta. \tag{21}$$

The equation of state for FCC particles becomes as follows:

$$\frac{P}{\rho_s \epsilon_s \theta} = 1 + 2(1+e)\epsilon_s g_0 - (0.73\epsilon_s + 8.957\epsilon_s^2). \tag{22}$$

Figure 14 shows the comparison between the predicted dimensionless solid pressure $P/(\epsilon_s \rho_s \theta)$ and the experimental data as a function of solid-volume fraction. We see that the new equation of state derived based on the measured radial distribution function for FCC particles agrees with the independently measured particle pressure.

Campbell and Wang (1991) in their bubbling Geldart B fluidized-bed research had studied dense systems and found that the particle pressure divided by the particle density, as shown in Eq. 4, correlated all their data. However, since they did not measure the granular temperature, they correlated their data using the bubble diameter times the gravitational constant in place of the granular temperature θ.

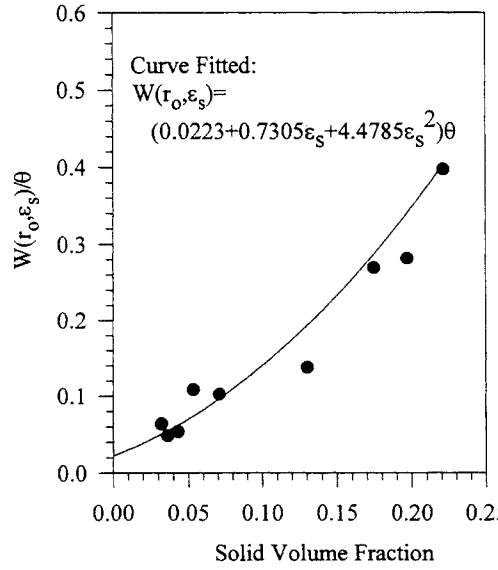

Figure 20. Variation of potential with solid-volume fraction for FCC particles.

Thermodynamics of Powder Flow

The analogy between the kinetic theory of granular flow and the kinetic theory of dense gases, suggested that the thermodynamics of powder flow can be constructed.

The internal energy of particles, U, per unit mass of particles can be obtained from the granular temperature, θ, depicted in Figure 13 (Gidaspow, 1994). This random translational energy is

$$U = \frac{3}{2}\theta, \tag{23}$$

where 3/2 corresponds to the specific heat at constant volume. Hence Figure 13 shows that the "acoustic"-type energy increases with particle loading and reaches a maximum near 5% particles by volume. The existence of this granular temperature implies the existence of entropy. Hence, by analogy with ordinary fluids for a one-component system, one can say that powders have the following fundamental equation for internal energy. Then, following the postulatory approach of Callen (1985), we have

$$U = U(S, \rho_B^{-1}), \tag{24}$$

where S is entropy and the bulk volume ρ_B^{-1} is the reciprocal of bulk density

$$\rho_B = \epsilon_s \rho_s. \tag{25}$$

The differential of energy is, as usual

$$dU = \left(\frac{\partial U}{\partial S}\right)_{\rho_B^{-1}} dS + \left(\frac{\partial U}{\partial \rho_B^{-1}}\right)_S d\rho_B^{-1}. \tag{26}$$

Then the definitions of granular temperature, θ, and pressure, p_s

$$\theta = \left(\frac{\partial U}{\partial S}\right)_{\rho_B^{-1}} \tag{27}$$

$$p_s = -\left(\frac{\partial U}{\partial \rho_B^{-1}}\right)_S \tag{28}$$

give the differential

$$dU = \theta dS - p_s d\rho_B^{-1}. \tag{29}$$

Rather than the fundamental Eq. 27, we need another function U that is a function of θ, as follows

$$U = U(\theta, \rho_B^{-1}). \tag{30}$$

Its differential is

$$dU = \left(\frac{\partial U}{\partial \theta}\right)_{\rho_B^{-1}} d\theta + \left(\frac{\partial U}{\partial \rho_B^{-1}}\right)_\theta d\rho_B^{-1}. \tag{31}$$

Equation 31 shows that the calculation of energy from the granular temperature, Eq. 23, assumed that the energy was not a function of the bulk density. But Eq. 31 and the analog of the Maxwell relation

$$\left(\frac{\partial S}{\partial \rho_B^{-1}}\right)_\theta = \left(\frac{\partial p_s}{\partial \theta}\right)_{\rho_B^{-1}} \tag{32}$$

show that

$$\left(\frac{\partial U}{\partial \rho_B^{-1}}\right) = \theta\left(\frac{\partial p_s}{\partial \theta}\right)_{\rho_B^{-1}} - p_s. \tag{33}$$

Substitution of the equation of state, Eq. 4, with a constant restitution coefficient (or e close to unity) shows that

$$\left(\frac{\partial U}{\partial \rho_B^{-1}}\right)_\theta = 0. \tag{34}$$

Hence the present kinetic theory of granular flow is restricted to the case when the energy is only a function of granular temperature. The gas law van der Waals equation shows that

$$\left(\frac{\partial U}{\partial \rho_B^{-1}}\right)_\theta = \frac{a}{\rho_B^{-2}}, \tag{35}$$

where the constant a is due to attractive cohesive forces. Hence a complete determination of the equation of state requires a measurement of solid pressure variation with granular temperature at a constant particle volume fraction. This may be done by the addition of flow agents, such as Cabosil or Tulenox, that decrease cohesion but do not change the collisional properties of particles.

Conclusions

Cohesive pressures for 75-μm FCC particles were obtained as a function of the volume fraction of particles from measurements of the radial distribution functions of statistical mechanics. Cohesion is near zero below 5% volume fraction of particles. It rises rapidly to about 70% of the ideal collisionless pressure at 25% volume fraction of solids.

When this cohesive pressure was subtracted from pressure given by the standard hard-sphere model, the corrected equation of state agreed with the measured solids pressure.

The derivative of this solids pressure with respect to the volume fraction allows one to calculate the pseudosonic velocity or the modulus of elasticity of particles. Such information is needed for computation of wave propagation in circulating fluidized beds and for prediction of particle and velocity distribution using hydrodynamic models.

Acknowledgment

This work was supported by National Science Foundation Grant Nos. CTS-9305850 and 9610053.

Notation

d_p = diameter of particle
F = force
r = radius
t = time
U_g = gas velocity
u_s = solid velocity
y = coordinate perpendicular to main flow direction
z = coordinate in the direction of flow
γ = shear rate
ϵ_s = solid volume fraction
μ_s = solid viscosity
ρ_s = density of solids
σ = standard deviation
σ^2 = variance

Literature Cited

Ahn, H., and C. Brennen, "Channel Flows of Granular Materials and their Rheological Implications," *Particulate Two-Phase Flow*, M. C. Roco, ed., Butterworth-Heinemann, Boston, p. 210 (1993).

Arastoopour, H., and Y. Yang, Experimental Studies on Dilute Gas and Cohesive Particles Flow Behavior Using Laser Doppler Anemometer," *Fluidization VII*, O. E. Potter and D. J. Nicklin, eds., Engineering Foundation, New York, p. 723 (1992).

Bagnold, R. A., "Experiments on a Gravity-Free Dispersion of Large Solid Spheres in a Newtonian Fluid Under Shear, *Proc. Roy. Soc.*, **A225**, 49 (1954).

Bahary, M., "Experimental and Computational Studies of Hydrodynamics in Two- and Three-Phase Fluidized Beds," PhD Thesis, IIT, Chicago (1994).

Balucani, U., and M. Zoppi, *Dynamics of Liquid State*, Oxford Science Publications, Oxford (1994).

Brady, J. F., "1994 Macroscopic Modeling of Viscous Suspension Flows," *Appl. Mech. Rev.*, **47**, 229 (1994).

Callen, H. B., *Thermodynamics and an Introduction to Thermostatistics*, Wiley, New York (1985).

Campbell, C. S., "The Stress Tensor for Simple Shear Flows of a Granular Material," *J. Fluid Mech.*, **203**, 409 (1989).

Campbell, C. S., and D. G. Wang, "A Particle Pressure Transducer Suitable for Use in Gas-Fluidized Beds," *Meas. Sci. Technol.*, **1**, 1275 (1990).

Campbell, C. S., and D. G. Wang, "Particle Pressure in Gas Fluidized Beds," *J. Fluid Mech.*, **227**, 495 (1991).

Campbell, C. S., and K. Rahman, "An Improved Particle Pressure Transducer," *Meas. Sci. Technol.*, **3**, 709 (1992).

Cao, J., and G. Ahmadi, "Gas-Particle Two-Phase Turbulent Flow in a Vertical Duct," *Int. J. Multiphase Flow*, **21**, 1203 (1995).

Carlos, C. R., and J. F. Richardson, "Solids Movement in Liquid Fluidized Beds—I Particle Velocity Distribution, *Chem. Eng. Sci.*, **23**, 813 (1968).

Carnahan, N. F., and K. E. Starling, "Equation of State for Nonattracting Rigid Spheres," *J. Chem Phys.*, **51**, 635 (1969).

Chapman, S., and T. G. Cowling, *The Mathematical Theory of Non-Uniform Gases*, 2nd ed., Cambridge Univ. Press, Cambridge (1961).

Chen, J. C., W. Polashenski, and K. Tuzla, "Normal Solid Stress in Fluidized Beds," AIChE Meeting, Preprint Vol. for Fluidization and Fluid-Particle Systems, San Francisco, p. 14 (1994).

Chu, X., A. D. Nikolov, and D. T. Wasan, "Effect of Particle Size and Polydispersity on the Depletion and Structural Forces in Colloidal Dispersions," *Langmuir*, **12**, 5004 (1996a).

Chu, X., A. D. Nikolov, and D. T. Wasan, "Effect of Interparticle Interactions on Stability, Aggregation and Sedimentation in Colloidal Suspensions," *Chem. Eng. Commun.*, **148**, 123 (1996b).

Cody, G. D., D. J. Goldfarb, G. V. Storch, and A. N. Norris, "Particle Granular Temperature in Gas Fluidized Beds," AIChE Meeting Preprint Vol. for Fluidization and Fluid-Particle Systems, Miami Beach, FL, p. 96 (1995).

Crowe, C. T., T. R. Troutt, and J. N. Chung, "Numerical Models for Two-Phase Turbulent Flows," *Annu. Rev. Fluid. Mech.*, **28**, 11 (1996).

Eaton, J. K., "Experiments and Simulations on Turbulence Modification by Dispersed Particles," *Appl. Mech. Rev.*, **47**, 44 (1994).

Egelstaff, P. A., *An Introduction to the Liquid State*, Academic Press, New York (1967).

Elghobashi, S. E., "On Predicting Particle-Laden Turbulent Flows," *Appl. Sci. Res.*, **52**, 309 (1994).

Elghobashi, S. E., and T. W. Abou-Arab, "A Two-Equation Turbulence Model for Two-Phase Flow," *Phys. Fluids*, **26**, 931 (1983).

Fan, L.-S., T. Kawamura, D. C. Chitester, and R. M. Kornosky, "Experimental Observation of Nonhomogeneity in a Liquid-Solid Fluidized Bed of Small Particles," *Chem. Eng. Commun.*, **37**, 141 (1985).

Gidaspow, D., *Multiphase Flow and Fluidization: Continuum and Kinetic Theory Description*, Academic Press, San Diego (1994).

Gidaspow, D., and L. Huilin, "Collisional Viscosity of FCC Particles in a CFB," *AIChE J.*, **42**, 2503 (1996a).

Gidaspow, D., and L. Huilin, "Liquid-Solid Fluidization Using Kinetic Theory," AIChE Meeting, Preprint Vol. for Fluidization and Fluid-Particle Systems, Chicago, p. 32 (1996b).

Gidaspow, D., L. Huilin, A. Neri, Y. Wu, and M. R. Mostofi, "Turbulence, Viscosity and Numerical Simulation of FCC Particles in CFB," Preprint Vol. for Fluidization and Fluid-Particle Systems, AIChE Meeting, Los Angeles, p. 58 (1997).

Gidaspow, D., M. Bahary, and Y. Wu, "Slurry Bubble Column Reactor Models Using Kinetic Theory," AIChE Meeting, Preprint Vol. for Fluidization and Fluid-Particle Systems, Miami Beach, FL, p. 164 (1995).

Glasser, B. J., I. G. Bevrekidis, and S. Sundaresan, "One- and Two-Dimensional Traveling Wave Solutions in Gas Fluidized Beds," *J. Fluid Mech.*, **306**, 183 (1996).

Gupta, R., "Dry Electrostatic Beneficiation of Illinois Coal and Eastern Oil Shales," PhD Thesis, Illinois Institute of Technology, Chicago (1990).

Gupta, R., D. Gidaspow, and D. T. Wasan, "Electrostatic Separation of Powder Mixture Based on the Work Functions of Its Constituents," *Powder Technol.*, **75**, 79 (1993).

Hail, J. M., and J. W. Mansoori, *Molecular-Based Study of Fluid*, American Chemical Society, Washington, D.C. (1983).

Hansen, J. P., and I. R. McDonald, *Theory of Simple Liquids*, Academic Press, San Diego (1991).

Hunter, R. J., *Foundation of Colloid Science II*, Oxford Science Publications, Oxford (1989).

Jackson, R., *Progress Toward a Mechanics of Dense Suspensions of Solid Particles*, AIChE Symp. Ser., **90**, 1 (1993).

Jaech, J. L., *Statistical Analysis of Measurement Errors*, Wiley, New York (1985).

Jenkins, J. T., and S. B. Savage, "A Theory for the Rapid Flow of Identical, Smooth, Nearly Elastic Particles," *J. Fluid Mech.*, **130**, 187 (1983).

Jenkins, J. T., and M. W. Richman, "Grad's 13-Moment System for a Dense Gas of Inelastic Sphere," *Arch. Rat. Mech. Anal.*, **87**, 355 (1985).

Johnson, P. C., and R. Jackson, "Frictional-Collisional Constitutive Relations for Granular Materials with Application to Plane Shearing," *J. Fluid Mech.*, **176**, 67 (1987).

Kumar, S., D. P. Hart, and C. E. Brennen, "Granular Pressure Measurements in Fluidized Beds," ASME Cavitation and Multiphase Flow Forum, Toronto, Ont., Canada (1990).

Leighton, D., and I. Rampall, "Measurement of the Shear-Induced Microstructure of Concentrated Suspensions of Non-Colloidal Spheres," *Particulate Two-Phase Flow*, M. C. Roco, ed., Butterworth-Heinemann, Boston, p. 195 (1993).

Louge, M. Y., E. Mastorakos, and J. T. Jenkins, "The Role of Particle Collisions in Pneumatic Transport," *J. Fluid Mech.*, **231**, 345 (1991).

Lun, C. K. K., S. B. Savage, D. J. Jeffrey, and N. Chepurniy, "Kinetic Theory for Granular Flow; Inelastic Particles in Coutte Flow and Slightly Inelastic Particles in a Granular Flowfield," *J. Fluid Mech.*, **140**, 223 (1984).

Lun, C. K. K., and S. B. Savage, "A Simple Kinetic Theory for Granular Flow of Rough, Inleastic Spherical Particles, *ASME E: J. Appl. Mech.*, **54**, 47 (1987).

Massoudi, M., and G. Ahmadi, "Rapid Flow of Granular Materials with Density and Fluctuation Energy Gradients," *Int. J. Non-linear Mech.*, **29**, 487 (1994).

Metropolis, N., A. W. Rosenbluth, M. N. Rosenbluth, A. H. Teller,

and E. Teller, "Equation of State Calculations by Fast Computing Machines," *J. Chem. Phys.*, **21**, 1087 (1953).
Meyer, S. L., *Data Analysis for Scientists and Engineers*, Wiley, New York (1975).
Miller, A., and D. Gidaspow, "Dense, Vertical Gas-Solid Flow in a Pipe," *AIChE J.*, **38**, 1801 (1992).
Miller, A., "Dense, Vertical Gas-Solid Flow in a Pipe," PhD Thesis, Illinois Institute of Technology, Chicago (1991).
Pita, J. A., and S. Sundaresan, "Developing Flow of a Gas-Particle Mixture in a Vertical Riser," *AIChE J.*, **39**, 541 (1993).
Phung, T. N., J. F. Brady, and G. Bossis, "Stokesian Dynamics Simulation of Brownian Suspensions," *J. Fluid Mech.*, **313**, 181 (1996).
Rhodes, M. J., "Modeling the Flow Structure of Upward Flowing Gas-Solid Suspensions, *Powder Technol.*, **60**, 27 (1990).
Richman, M. R., "The Source of Second Moments in Dilute Granular Flows of Highly Inelastic Spheres," *J. Rheol.*, **33**, 1293 (1989).
Rogers, C. B., and J. K. Eaton, "The Effect of Small Particles on Fluid Turbulence in a Flat-Plate, Turbulent Boundary Layer in Air," *Phys. Fluids A. Fluid Dyn.*, **3**, 928 (1991).
Samuelsberg, A., and B. J. H. Hjertager, "Computational Modeling of Gas/Particle Flow in a Riser, *AIChE J.*, **42**, 1536 (1996).
Sangani, A. S., G. Mo, H.-K Tsao, and D. L. Koch, "Simple Shear Flows of Dense Gas-Solid Suspensions at Finite Stokes Numbers," *J. Fluid Mech.*, **313**, 309 (1996).
Savage, S. B., and D. J. Jeffrey, "The Stress Tenser in a Granular Flow at High Shear Rates," *J. Fluid Mech.*, **110**, 255 (1981).
Savage, S. B., "Granular Flows at High Shear Rate," *Theory of Dispersed Multiphase Flow*, R. E. Meyer, ed., Academic Press, New York (1983).
Savage, S. B., "Streaming Motions in a Bed of Vibrationally Fluidized Dry Granular Material," *J. Fluid Mech.*, **194**, 457 (1988).
Shao, S., H. J. Slovik, and H. Arastoopour, "The Flight Time Technique for Simultaneous Measurements of Particle Flow Parameters Using a Laser Doppler Anemometer (LDA)," *Fluidization VIII*, C. Laguerie and J. F. Large, eds., Engineering Foundation, France, p. 201 (1995).
Simonin, O., E. Deutsch, and J. P. Minier, "Eulerian Prediction of the Fluid/Particle Correlated Motion in Turbulent Two-Phase Flows," *Appl. Sci. Res.*, **51**, 275 (1993).
Sinclair, J. L., and R. Jackson, "Gas-Particle Flow in a Vertical Pipe with Particle-Particle Interaction," *AIChE J.*, **35**, 1473 (1989).
Sommerfeld, M., "Modelling of Particle-Wall Collisions in Confined Gas-Particle Flows," *Int. J. Multiphase Flow*, **18**, 905 (1992).
Squires, A. M., M. Kwauk, and A. A. Avidan, "Fluid Beds: At Last, Challenging Two Entrenched Practices," *Science*, 230, 1329 (1985).
Tanaka, T., T. Kawaguchi, and Y. Tsuji, "Discrete Particle Simulation of Flow Patterns in Two-Dimensional Gas Fluidized Beds," *Int. J. Mod. Phys. B*, **7**, 1889 (1993).
Temperley, H. N. V., J. S. Rowlinson, and G. S. Rushbrooke, *Physics of Simple Liquids*, North-Holland, Amsterdam (1968).
Tsao, H.-K., and D. L. Koch, "Simple Shear Flows of Dilute Gas-Solid Suspensions," *J. Fluid Mech.*, **296**, 211 (1995).
Tsuji, Y., T. Kawaguchi, and T. Tanaka, "Discrete Particle Simulation of Two-Dimensional Fluidized Bed," *Powder Technol.*, **77**, 79 (1993).
Viollet, P. L., and O. Simonin, "Modeling Dispersed Two-Phase Flows: Closure, Validation and Software Development," *Appl. Mech. Rev.*, **47**, 80 (1994).
Walton, O. R., and R. L. Braun, "Stress Calculations for Assemblies of Inelastic Spheres in Uniform Shear," *Acta Mech.*, **63**, 73 (1986).
Walton, O. R., "Numerical Simulation of Inelastic Frictional Particle-Particle Interactions," *Particulate Two-Phase Flow*, M. C. Roco, ed., Butterworth-Heinemann, Boston, p. 884 (1993).
Wasan, D. T., W. Xu, A. D. Nikolov, and X. Chu, "Role of Depletion and Surface-Induced Structural Forces in Fine Particle Separations," World Congr. of Chemical Engineering, San Diego, CA (1996).
Xu, W., A. D. Nikolov, and D. T. Wasan, "Structure and Stability of Food Emulsions as Probed by the Kossel Diffraction Technique," Ann. Meeting of the American Institute of Chemical Engineers, Chicago (1996).
Yonemura, S., T. Tanaka, and Y. Tsuji, "Cluster Formation in Gas-Solid Flow Predicted by the DSMC Method, ASME Gas-Solid Flows, **166**, 303 (1993).
Yoshida, H., K. Ito, and N. Ise, "Microscopic Observation and Quasielastic Light-Scattering Measurements of Colloid Crystals: Determination of the Radial Distribution Function and Structure Factor for the Two-State Structure," *J. Amer. Chem. Soc.*, **112**, 592 (1990).

Appendix A: Estimate of Restitution Coefficient

From our measurements of granular temperature and solid-volume fraction profile in the dilute regime, obtained using the CCD camera, we estimated the particle-plastic wall restitution coefficient (see Figure A1). We used the formula of Johnson and Jackson (1987), as shown in Figure A1:

$$\theta_w = 0.153 \frac{d_p}{\epsilon_s(1-e_w^2)} \frac{d\theta}{dr_w}. \tag{A1}$$

We obtain a value of $e_w = 0.96$. Since the wall, made of plastic, is softer than the FCC particles, the value of $e = 1-10^{-4}$ estimated by Gidaspow (1994) is reasonable.

We also computed the restitution coefficient based on the formula of Louge et al. (1991):

$$\mu_f = \frac{5\sqrt{\pi}\, d_p}{96\epsilon_{s,w}\left(1+\frac{\lambda}{R}\right)\sqrt{\theta_w}} \frac{dv}{dr} \tag{A2}$$

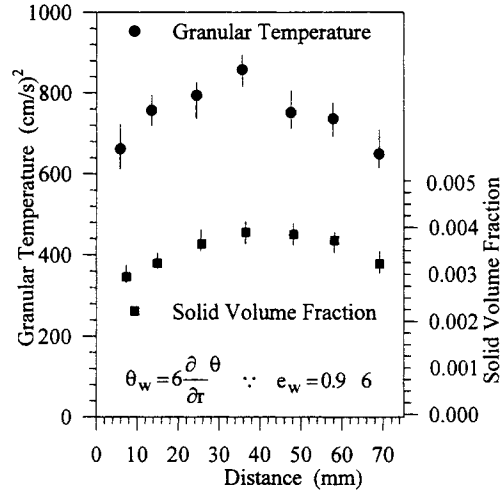

Figure A1. Boundary condition for granular temperature wall boundary condition (Johnson and Jackson, 1987): Granular flux = Dissipation at the wall

$$\theta_W = \left(0.153 \frac{d_p}{\epsilon_s}\right) \times \frac{1}{1-e_w^2} \frac{\partial\theta}{\partial r}.$$

$$\frac{25\sqrt{\pi\theta_s}d_p}{128\left(1+\frac{\lambda}{R}\right)}\frac{d\theta}{dr}$$

$$=\frac{3}{8}\epsilon_{s,w}\theta_w\sqrt{3\theta_w}\left[\frac{7}{2}(1+e_w)\mu_f^2-(1-e_w)\right]. \quad \text{(A3)}$$

We obtain a value of $\mu_f = 0.298$ and $e_w = 0.719$ that is in the range of the authors' recommendations.

Appendix B: Analysis of Measurement Errors

Solid volume fraction

In this study, the solid-volume fraction was measured by an X-ray densitometer. Figure B1 shows the time-averaged solid-volume fractions and their error range measured by the X-ray densitometer. As a comparison, we also measured the solid-volume fraction using our CCD camera technique. Such methods were first used by Fan et al. (1985) to determine the solid-volume fraction in the solid–liquid fluidized bed. Figure B2 shows the average solid-volume fractions and their error range at the same test condition as the X-ray densitometer. Figure B3 shows the comparison of the solid-volume fraction measured by the X-ray densitometer with the CCD camera technique. The agreement between the two measuring techniques is quite reasonable.

Granular temperature

Figure B4a, B4b, and B4c show the particle speed and the velocity distributions for two different sample sizes. In these figures, the coordinate represents the fraction at which particle velocities fell into the velocity interval. Figure B5 shows the granular temperature deviations for two measuring times.

Measurement errors

The variances of measured particle solid-volume fractions σ_{ϵ_s}, pressure σ_{p_s}, and granular temperature σ_θ are as follows

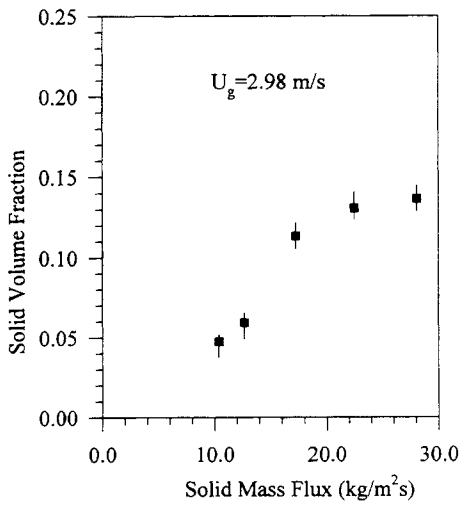

Figure B1. Solid-volume fractions measured with the X-ray densitometer.

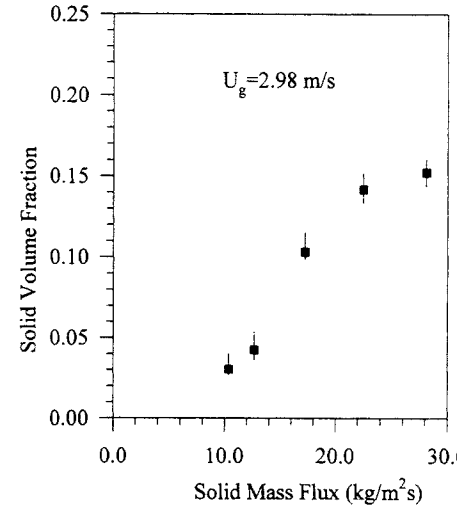

Figure B2. Solid volume fractions measured with the CCD camera.

(Meyer, 1975; Jaech, 1985):

$$\sigma_{p_s}^2 = \sum_{i=1}^{n}\frac{(p_{s,i}-\bar{p}_s)^2}{n} = 13.36 \text{ (Pa)} \quad \text{(B1)}$$

$$\sigma_\theta^2 = \sum_{i=1}^{n}\frac{(\theta_i-\bar{\theta})^2}{n} = 0.1029 \quad (\text{m/s})^2 \quad \text{(B2)}$$

$$\sigma_{\epsilon_s}^2 = \sum_{i=1}^{n}\frac{(\epsilon_{s,i}-\bar{\epsilon}_s)^2}{n} = 0.00618, \quad \text{(B3)}$$

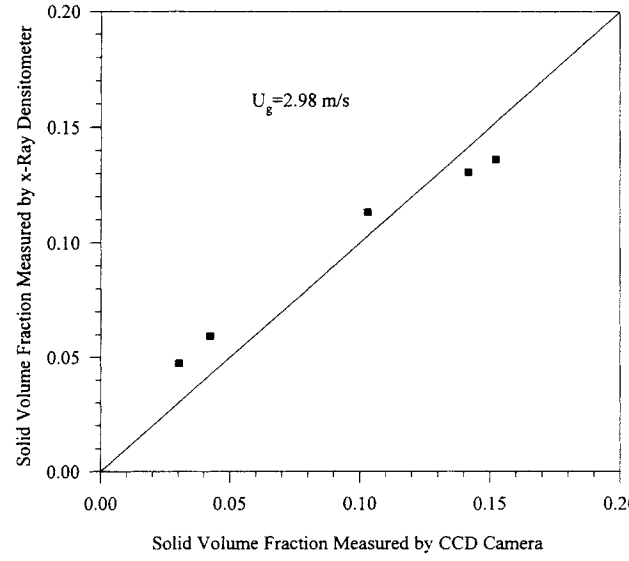

Figure B3. A comparison of solid-volume fractions measured with X-ray densitometer and CCD camera.

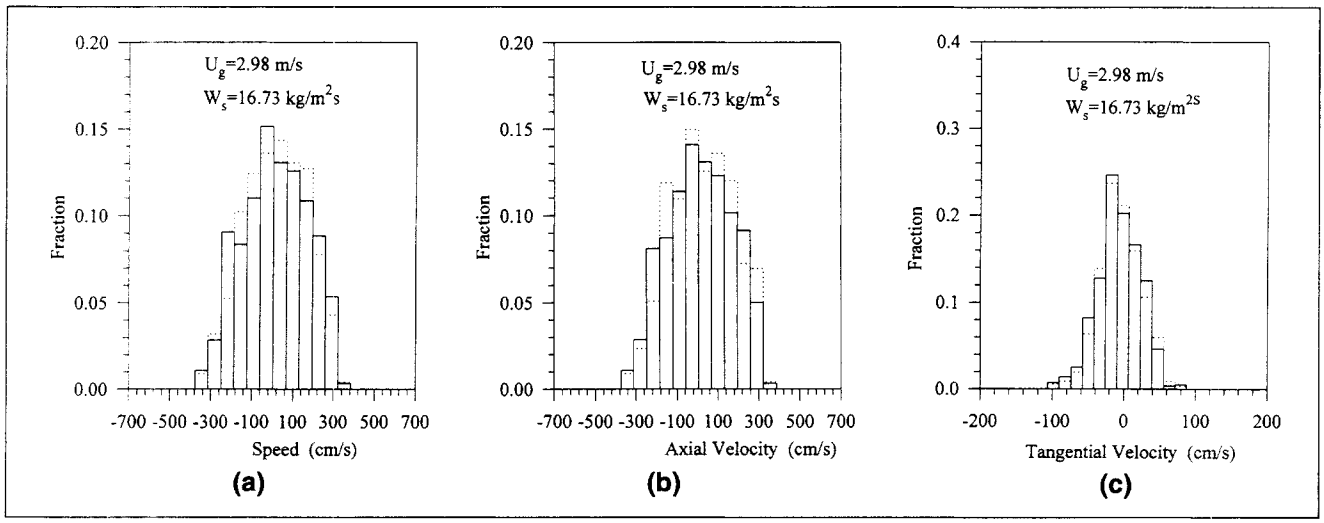

Figure B4. (a) Particle speed distribution (-----N = 140; mean value = −20.15 cm/s; standard deviation = 186.01 cm/s: ---N = 261; mean value = −14.43 cm/s; standard deviation = 191.83 cm/s); (b) Particle axial velocity distribution (-----N = 140; mean value = −20.97 cm/s; standard deviation = 183.51 cms: ---N = 261; mean value = −14.96 cm/s; standard deviation = 189.57 cm/s); (c) Particle tangential velocity distribution (-----N = 140; mean value = −0.97 cm/s; standard deviation = 30.05 cm/s; ---N = 261; mean value = −0.82 cm/s; standard deviation = 29.01 cm/s).

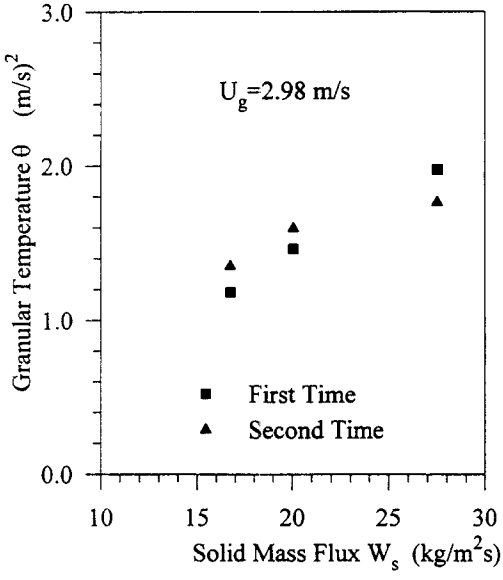

Figure B5. Granular temperature duplicate measurements.

where subscript i represents the number of samples in each case and the overbar represents the average values in each case. The relative error of particle pressure, ϵ_{p_s}, granular temperature, ϵ_θ, and solid volume fraction, ϵ_{ϵ_s}, are

$$\epsilon_{p_s} = \frac{1}{n}\sum_{i=1}^{n}\left(\frac{p_{s,i} - \bar{p}_s}{\bar{p}_s}\right) = 14.36\% \tag{B4}$$

$$\epsilon_\theta = \frac{1}{n}\sum_{i=1}^{n}\left(\frac{\theta_i - \bar{\theta}}{\bar{\theta}}\right) = 12.26\% \tag{B5}$$

$$\epsilon_{\epsilon_s} = \frac{1}{n}\sum_{i=1}^{n}\left(\frac{\epsilon_{s,i} - \bar{\epsilon}}{\bar{\epsilon}}\right)^2 = 8.14\%. \tag{B6}$$

The total of relative error is

$$\epsilon_{\frac{p_s}{\epsilon_s\theta}} = \left(\epsilon_{p_s}^2 + \epsilon_{\epsilon_s}^2 + \epsilon_\theta^2\right)^{0.5} = 20.56\%. \tag{B7}$$

Manuscript received Apr. 21, 1997, and revision received Sept. 8, 1997.